The Astrophysical Journal, 811:83 (7pp), 2015 October 1 doi:10.1088/0004-637X/811/2/83
© 2015. The American Astronomical Society. All rights reserved.

MODELING THE MULTI-BAND AFTERGLOW OF GRB 091127: EVIDENCE OF A HARD ELECTRON ENERGY SPECTRUM WITH AN INJECTION BREAK

Qiang Zhang[1,2], Yong-Feng Huang[3,4], and Hong-Shi Zong[1,2,5]
[1] Department of Physics, Nanjing University, Nanjing 210093, China; zonghs@nju.edu.cn
[2] Joint Center for Particle, Nuclear Physics and Cosmology, Nanjing 210093, China
[3] School of Astronomy and Space Science, Nanjing University, Nanjing 210093, China; hyf@nju.edu.cn
[4] Key Laboratory of Modern Astronomy and Astrophysics (Nanjing University), Ministry of Education, Nanjing 210093, China
[5] State Key Laboratory of Theoretical Physics, Institute of Theoretical Physics, CAS, Beijing, 100190, China
Received 2015 July 5; accepted 2015 August 15; published 2015 September 24

ABSTRACT

The afterglows of gamma-ray bursts (GRBs) are believed to originate from the synchrotron emission of shock-accelerated electrons produced by the interaction between the outflow and the external medium. The accelerated electrons are usually assumed to follow a power-law energy distribution with an index of p. Observationally, although most GRB afterglows have a p larger than 2, there are still a few GRBs suggestive of a hard ($p < 2$) electron spectrum. The well-sampled broad-band afterglow data for GRB 091127 show evidence of a hard electron spectrum and strong spectral evolution, with a spectral break moving from high to lower energies. The spectral break evolves very fast and cannot be explained by the cooling break in the standard afterglow model, unless evolving microphysical parameters are assumed. In addition, the multi-band afterglow light curves show an achromatic break at around 33 ks. Based on the model of a hard electron spectrum with an injection break, we interpret the observed spectral break as the synchrotron frequency corresponding to the injection break, and the achromatic break as a jet break caused by the jet-edge effect. It is shown that the spectral evolution and the multi-band afterglow light curves of GRB 091127 can be well reproduced by this model.

Key words: acceleration of particles – gamma-ray burst: individual (GRB 091127) – ISM: jets and outflows

1. INTRODUCTION

Gamma-ray bursts (GRBs) are the most energetic stellar explosions in the universe; they produce a short prompt γ-ray emission followed by a multi-band afterglow that can be observed up to several years. The afterglows of GRBs are believed to originate from the synchrotron emission of shock-accelerated electrons produced by the interaction between the outflow and the external medium (Rees & Mészáros 1992; Mészáros & Rees 1993, 1997; Sari et al. 1998; Chevalier & Li 2000). When the blast wave enters a self-similar phase described by the Blandford–McKee self-similar solution (Blandford & McKee 1976), the hydrodynamics are mainly determined by six free parameters, i.e., the total energy of the blast wave E, the jet half-opening angle θ_j, the fractions of shock energy carried by electrons and magnetic fields (ϵ_e and ϵ_B), the ambient density n, and the electron spectral index p. The temporal and spectral indices of the afterglow emission are largely determined by the electron spectral index p, which is dependent only on the underlying micro-physics of the acceleration process.

Particle acceleration is usually attributed to the *Fermi* process (Fermi 1954), in which particles bounce back and forth across the shock to gain energy. Particles accelerated by this mechanism follow a power-law energy distribution $N(E)dE \propto E^{-p}dE$, with a cutoff at high energies. Some analytical and numerical studies indicate a nearly universal spectral index of $p \sim 2.2$–2.4 (Bednarz & Ostrowski 1998; Kirk et al. 2000; Achterberg et al. 2001; Lemoine & Pelletier 2003; Spitkovsky 2008), though other studies suggest that there is a large range of possible values for p of 1.5–4 (Baring 2004). Observationally, the value of p can be estimated from the spectral analysis of the multi-band afterglow (Chevalier & Li 2000; Panaitescu & Kumar 2002; Starling et al. 2008; Curran et al. 2009) or the X-ray data alone (Shen et al. 2006; Curran et al. 2010). Both studies, however, show that the observed values of p are inconsistent with a single universal value, but show a rather wide distribution.

Moreover, observations of some GRB afterglows suggest a hard electron spectrum with an index $p < 2$ (Panaitescu & Kumar 2001a). GRB 010222 was one of the first afterglows seen with such a hard electron spectrum (Masetti et al. 2001; Stanek et al. 2001); this motivated theoretical studies in that direction (Bhattacharya 2001; Dai & Cheng 2001; Huang et al. 2006; Resmi & Bhattacharya 2008). Different hard-spectrum models were assumed to explain the afterglow of GRB 010222 (Cowsik et al. 2001; Sagar et al. 2001; Panaitescu & Kumar 2002; Bhattacharya & Resmi 2004; Resmi & Bhattacharya 2008), though other explanations, e.g., continuous energy injection (Björnsson et al. 2002), could also reproduce the observed evolution of this afterglow. Other GRB afterglows, e.g., GRB 020813 (Butler et al. 2003; Covino et al. 2003), GRB 041006 (Misra et al. 2005), showing similar characteristics could also be explained with a hard electron spectrum (Resmi & Bhattacharya 2008).

For a hard electron spectrum, a cutoff at the high-energy end is required to keep the total energy from diverging. The theories of a hard electron spectrum can be divided into two categories by and large. One kind of model assumes that a hard electron energy distribution can extend to a maximum electron Lorentz factor γ_M, beyond which there is an exponential cutoff (Bhattacharya 2001; Dai & Cheng 2001). The other kind of model assumes that a hard electron spectrum terminates at some electron Lorentz factor γ_b, above which the electron distribution steepens to another power law with an index $p > 2$ (Panaitescu & Kumar 2001b; Bhattacharya & Resmi 2004; Resmi & Bhattacharya 2008; Wang et al. 2012). In this paper, we call γ_b an "injection break" as in Bhattacharya & Resmi

(2004) and Resmi & Bhattacharya (2008). The evolution of $\gamma_{\rm M}$ or $\gamma_{\rm b}$ has so far not been well understood, and different expressions were assumed in the literature. We distinguish between these two kinds of models by naming them the "single power-law hard spectrum (SPLH)" model and the "double power-law hard spectrum (DPLH)" model, respectively.

Although some GRB afterglows could be well explained by the hard-spectrum model (Resmi & Bhattacharya 2008), we should note that all the afterglows referred to above show a shallow-to-steep decay in the optical and/or X-ray light curves, with an initial decay slope ∼0.5–0.8 steepening to ∼1.3–1.4 at around 0.5 day, and the optical/X-ray spectral indices are in the range of ∼0.6–1.0 (Resmi & Bhattacharya 2008). These characteristics, however, are ubiquitous among the canonical afterglow light curves observed in the era of *Swift* (Nousek et al. 2006; Zhang et al. 2006), and the shallow decays are usually explained by assuming continuous energy injection to the decelerating blast wave in the case of $p > 2$(Dai & Lu 1998; Rees & Mészáros 1998; Sari & Mészáros 2000; Zhang & Mészáros 2001). Therefore, the explanation of a hard electron spectrum seems to be dubious and can be confused with the continuous energy injection model especially when the spectral information is missing (Kumar & Zhang 2015).

GRB 091127, at a redshift of $z = 0.49$ (Cucchiara et al. 2009; Thöne et al. 2009), has high-quality broad-band afterglow data (Filgas et al. 2011; Troja et al. 2012). These data allow us to test several proposed emission models and outflow characteristics in unprecedented detail. The broad-band spectral energy distribution (SED) of the afterglow shows evidence of a hard electron spectrum and strong spectral evolution, with a break frequency moving from high to lower energies. Based on the SPLH model with a spectral index of $p = 1.5$, Filgas et al. (2011) interpreted this spectral break as the cooling break in the case of a homogeneous interstellar medium (ISM) circumburst environment. However, the observed spectral break evolves much faster ($\propto t^{-1.23}$) than the cooling break ($\propto t^{-1/2}$). To solve this problem, some microphysical parameters (e.g., $\epsilon_{\rm B}$) were required to evolve with time. Indeed, modifications of the standard afterglow model with evolving microphysical parameters ($\epsilon_{\rm e}$ or/and $\epsilon_{\rm B}$) have been proposed to explain the X-ray afterglow plateaus (Ioka et al. 2006), chromatic light-curve breaks (Panaitescu et al. 2006), afterglow rebrightenings (Kong et al. 2010), or some other difficulties encountered with observations (van der Horst et al. 2014). So far, a complete knowledge of the microphysical processes is still lacking. How a parameter evolves mainly depends on which phenomenon needs to be explained, and sometimes the evolution of $\epsilon_{\rm e}$ and $\epsilon_{\rm B}$ would have to match with certain observations, which makes this scenario seem ad hoc and contrived (Panaitescu et al. 2006).

Based on the DPLH model proposed by Resmi & Bhattacharya (2008), we show in this paper that the observed spectral break can be well explained by the injection break frequency $\nu_{\rm b}$ and the observed spectral evolution is the result of $\nu_{\rm b}$ crossing the optical/NIR bands. Previous studies usually assume $\nu_{\rm b}$ to be above the X-ray band even at late times (Panaitescu & Kumar 2002; Resmi & Bhattacharya 2008), thus the spectral evolution caused by $\nu_{\rm b}$ could not be observed. Therefore, with the high-quality afterglow data of GRB 091127, it may be the first time we see the evolution of the injection break in a hard electron spectrum.

Our paper is organized as follows. We summarize the observational facts of GRB 091127 in Section 2. The model of a double power-law electron spectrum is described in Section 3. In Section 4, we constrain the free parameters in this model and fit the multi-band afterglow light curves. Finally, we sum up our results and give a brief discussion in Section 5. Throughout the paper, the convention $F_\nu \propto \nu^{-\beta}t^{-\alpha}$ is followed, and we use the standard notation $Q_x = Q/10^x$ with Q being a generic quantity in cgs units. We also assume a concordance cosmology of $H_0 = 71\ {\rm km\ s^{-1}\ Mpc^{-1}}$, $\Omega_{\rm M} = 0.27$, $\Omega_\Lambda = 0.23$. All the quoted errors are given at a 1σ confidence level.

2. OBSERVATIONAL FACTS

GRB 091127 triggered the *Swift*/BAT at 23:25:45 UT on 2009 November 27 (Troja et al. 2009) and was also observed by *Konus/WIND*, *Suzaku*, and *Fermi*/GBM. The measured duration of T_{90} in the 15–350 keV band is 7.1 ± 0.2 s (Stamatikos et al. 2009). The time-averaged spectrum is adequately fit by a Band function (Band et al. 1993) with $E_{\rm peak} = 45 \pm 3$ keV, $\alpha = -1.37 \pm 0.07$, $\beta = -2.31 \pm 0.03$, and the total fluence in the 8–1000 keV energy range is $(1.9 \pm 0.2) \times 10^{-5}\ {\rm erg\ cm^{-2}}$ (Troja et al. 2012). With a redshift of $z = 0.49$, the isotropic equivalent energy of GRB 091127 is $E_{\gamma,{\rm iso}} = (1.1 \pm 0.1) \times 10^{52}$ erg (Troja et al. 2012). In addition, GRB 091127 is an event associated with SN 2009nz (Cobb et al. 2010).

2.1. X-Ray Afterglow

Due to an Earth limb constraint, *Swift*/XRT started to follow up on GRB 091127 about 53 minutes after the BAT trigger (Evans et al. 2009b), and the X-ray observations continued for around 50 days. The X-ray spectra were fitted with an absorbed power law, with a photon index of $\Gamma_{\rm X} \sim 1.8$, and a host absorbing column density of $N_{\rm H} \sim 1.3 \times 10^{21}\ {\rm cm^{-2}}$ (Filgas et al. 2011). The X-ray light curve could be described by a smoothly broken power-law model (Beuermann et al. 1999) with an initial decay slope $\alpha_{\rm X,1} = 1.02 \pm 0.04$ steepening to $\alpha_{\rm X,2} = 1.61 \pm 0.04$ at the break time $t_{\rm bk} \approx 33$ ks (Filgas et al. 2011). Similar results were given by Troja et al. (2012).

2.2. Optical Afterglow

The optical afterglow of GRB 091127 was monitored by *Swift*/UVOT, the 2 m Liverpool Telescope (LT), the Faulkes Telescope South (FTS), SkycamZ, and the Gamma-ray burst Optical Near-infrared Detector (GROND) (Filgas et al. 2011; Troja et al. 2012). LT began observing the burst 141 s after the BAT trigger and located the position of the transient at R.A. (J2000) $= 02^{\rm h}26^{\rm m}19\overset{\rm s}{.}89$, and decl.(J2000) $= -18°57'08\overset{''}{.}6$ (uncertainty of $0\overset{''}{.}5$; Smith et al. 2009). GROND started observations 58 minutes after the trigger with very high-quality data in the optical/NIR bands (Updike et al. 2009). Using the well-sampled NIR/optical data obtained with GROND, Filgas et al. (2011) gave a detailed study of the multi-color light curves and the broad-band SEDs from NIR to X-rays. We summarize their main results in the following.

The optical/NIR light curves are also well fitted with a smoothly broken power law after subtracting the supernova (SN) bump at late times. The initial decay slopes are slightly different among the optical bands, ranging from 0.32 to 0.43. The average value is $\alpha_{\rm opt,1} = 0.38 \pm 0.04$, then steepens to $\alpha_{\rm opt,2} \sim 1.6$ at a break time of around 33 ks. The decay of the

NIR light curves is slightly shallower but with larger inaccuracies compared with that of optical bands because the fitting is affected by the somewhat lower signal-to-noise ratio of the NIR data (Filgas et al. 2011). The most notable feature is the strong spectral evolution in the optical/NIR bands, the spectral index $\beta_{\rm opt/NIR}$ rises from $\sim$0.23 to $\sim$0.80 between 3 and 300 ks. The broad-band SEDs before $\sim$110 ks could be fitted with a smoothly broken power-law when $\beta_{\rm opt/NIR} = \beta_{\rm X} - 0.5$ was fixed. The derived high-energy spectral index is $\beta_{\rm X} = 0.75 \pm 0.004$. The break frequency decreases from $\sim$28.7 to $\sim$0.3 eV and could be fitted to scale as $\propto t^{-1.23\pm0.06}$. The SEDs at later times are consistent with a simple power law, and the spectral indices in the optical/NIR bands are in agreement with that of X-ray afterglow within 1σ errors. The SEDs require the break frequency to cross the optical bands, which results in the spectral evolution and very smooth breaks in the optical/NIR light curves. Fits of the optical/NIR data alone as well as the broad-band SEDs imply no host dust extinction.

Troja et al. (2012) studied the multi-band afterglow of GRB 091127 using the X-ray data from *Swift*/XRT and *Chandra* and the optical data from UVOT, LT, FTS, and SkycamZ. The optical light curves show a gradual shallow-to-steep decay at around 30 ks as well. Their obtained decay slopes are slightly different from those given by Filgas et al. (2011), mainly because they fitted the light curves with a triple broken power law. They also found a spectral break evolution with a decay index of -1.5 ± 0.5. However, the sparse sampling in the optical bands forbade them to derive the detailed evolution of the spectral index and break frequency as done by Filgas et al. (2011).

3. MODEL

The afterglow of GRB 091127 shows two important properties: the spectral evolution in the optical/NIR bands and the achromatic break at around 33 ks in both X-ray and optical/NIR light curves. Moreover, a hard electron spectrum is required due to the flat spectrum in the optical/NIR band at early times. Based on the DPLH model and using the assumed evolution function of the injection break proposed by Bhattacharya (2001) and Resmi & Bhattacharya (2008), we interpreted the observed spectral evolution as the injection break frequency $\nu_{\rm b}$ crossing the optical/NIR bands, and we explain the achromatic break as a jet break due to the jet-edge effect (Mészáros & Rees 1999) as proposed by Filgas et al. (2011) and Troja et al. (2012). Therefore, the multi-band afterglow of GRB 091127 is a joint result of the spectral evolution caused by the injection break and the jet-edge effect. In the following, we give a brief description of the DPLH model and present the useful formula which will be used in Section 4 (see Resmi & Bhattacharya 2008 for more details).

The double-slope electron energy distribution with slopes p_1 and p_2 is represented as (Resmi & Bhattacharya 2008; Wang et al. 2012)

$$N(\gamma_{\rm e}) = C_{\rm e}\begin{cases}\left(\dfrac{\gamma_{\rm e}}{\gamma_{\rm b}}\right)^{-p_1}, & \gamma_{\rm m} < \gamma_{\rm e} < \gamma_{\rm b},\\ \left(\dfrac{\gamma_{\rm e}}{\gamma_{\rm b}}\right)^{-p_2}, & \gamma_{\rm b} < \gamma_{\rm e} < \gamma_{\rm M},\end{cases} \quad (1)$$

where $C_{\rm e}$ is the normalization constant, $\gamma_{\rm m}$ and $\gamma_{\rm M}$ are minimum and maximum electron Lorentz factors, respectively, and $\gamma_{\rm b}$ is the injection break. The electron spectral indices $1 < p_1 < 2$, $p_2 > 2$. The definition of $\gamma_{\rm M}$ is unimportant and can be set to infinity (Resmi & Bhattacharya 2008). The physical origin of $\gamma_{\rm b}$ is not clear, but one can simply assume that it is a function of γ alone (Bhattacharya 2001; Resmi & Bhattacharya 2008),

$$\gamma_{\rm b} = \xi(\beta\gamma)^q, \quad (2)$$

where ξ is a constant of proportionality, $\beta = \sqrt{1-\gamma^{-2}}$ is the dimensionless bulk velocity, and q is assumed to be a constant for simplicity.

According to this electron energy distribution and the jump conditions for a relativistic shock, the electron number density and energy density of the shocked medium can be written as two integrals: $\int_{\gamma_{\rm m}}^{\gamma_{\rm M}} N(\gamma_{\rm e})d\gamma_{\rm e} = 4\gamma n(r)$ and $\int_{\gamma_{\rm m}}^{\gamma_{\rm M}} N(\gamma_{\rm e})\gamma_{\rm e} m_{\rm e} c^2 d\gamma_{\rm e} = 4\gamma(\gamma-1)n(r)m_{\rm p}c^2\epsilon_{_e}$, from which one obtains the minimum Lorentz factor,

$$\gamma_{\rm m} = \left(f_{\rm p}\frac{m_{\rm p}}{m_{\rm e}}\frac{\epsilon_{\rm e}}{\xi^{2-p_1}}\right)^{\frac{1}{p_1-1}}\beta^{-\frac{q(2-p_1)}{p_1-1}}(\gamma-1)^{\frac{1}{p_1-1}}\gamma^{-\frac{q(2-p_1)}{p_1-1}}, \quad (3)$$

where $f_{\rm p} = \dfrac{(2-p_1)(p_2-2)}{(p_1-1)(p_2-p_1)}$.

We calculate the break frequencies of synchrotron spectra $\nu_{\rm m}$, $\nu_{\rm b}$, $\nu_{\rm c}$ and the peak flux $F_{\nu,\rm max}$ according to the formula given by Wijers & Galama (1999):

$$\nu_{\rm m} = \frac{x_{\rm p}}{1+z}\frac{q_{\rm e}B'}{\pi m_{\rm e}c}\gamma\gamma_{\rm m}^2, \quad (4)$$

$$\nu_{\rm b,c} = \frac{0.286}{1+z}\frac{q_{\rm e}B'}{\pi m_{\rm e}c}\gamma\gamma_{\rm b,c}^2, \quad (5)$$

$$F_{\nu,\rm max} = \frac{\phi_{\rm p}q_{\rm e}^3(1+z)}{\sqrt{3}\,m_{\rm e}c^2d_{\rm L}^2}B'\gamma r^3 n, \quad (6)$$

where $q_{\rm e}$ is the electron charge, $B' = \left(32\pi n m_{\rm p}c^2\epsilon_{\rm B}\right)^{1/2}\gamma$ is the post-shock magnetic field density, $d_{\rm L}$ is the luminosity distance corresponding to the redshift z, $\gamma_{\rm c} = 6\pi m_{\rm e}c/(\sigma_{\rm T}\gamma B'^2 t)$ is the cooling Lorentz factor of electrons. $x_{\rm p}$ and $\phi_{\rm p}$ are the dimensionless peak frequency and the peak flux, respectively. Their dependence on p can be obtained from Wijers & Galama (1999).

The calculation of break frequencies and peak flux given above depends on the hydrodynamic evolution of the shock. As the achromatic break at $t_{\rm bk}$ in the light curves of GRB 091127 is suggestive of a jet break, it is necessary to analyze its physical origin at first, which determines our treatment of the hydrodynamic evolution. A jet-break-like steepening in the light curves could be due to two effects. The first is the jet-edge effect happening at $\gamma \sim 1/\theta_{\rm j}$, after which the light curves have a steepening by $t^{-3/4}$ (or $t^{-1/2}$) for an ISM (or wind) medium (Mészáros & Rees 1999). This effect does not change the hydrodynamic evolution. The second effect is caused by sideways expansion, which has important effects on the hydrodynamics when $\gamma < 1/\theta_{\rm j}$ is satisfied. The flux after the

jet break decays as t^{-p} for a normal electron spectrum with index $p > 2$ (Rhoads 1999; Sari et al. 1999). For a hard electron spectrum ($1 < p < 2$), however, the decay slope after this kind of jet break is somewhat different (Dai & Cheng 2001; Wang et al. 2012).

Nevertheless, numerical simulations and more sophisticated analytical treatments suggest that the sideways expansion of a relativistic jet is unimportant until γ drops below $\sim$2 (Huang et al. 2000; Granot et al. 2001; Kumar & Granot 2003; Cannizzo et al. 2004; Zhang & MacFadyen 2009; de Colle et al. 2012; Granot & Piran 2012; van Eerten et al. 2012). Moreover, using the expression (their Equation (11)) given by Wang et al. (2012) who considered the effect of sideways expansion, the predicted decay slope of the light curves of GRB 091127 after $t_{\rm bk}$ is ~ -2.4 (when the parameters given in Section 4 were used), which is much steeper than the observed. Therefore, we neglect the effect of sideways expansion on the hydrodynamic evolution in the relativistic phase.

Using the light curve decay indices given by Resmi & Bhattacharya (2008), a wind-like circumburst medium can be easily excluded. So here we only consider the ISM case. For simplicity, we consider the self-similar evolution of a spherical blast wave in the adiabatic case (Blandford & McKee 1976). The radius r and bulk Lorentz factor γ evolve as $r(t) = \left[17Et/4\pi nm_{\rm p}c(1+z)\right]^{1/4}$ and $\gamma(t) = \left[17E(1+z)/1024\pi nm_{\rm p}c^5t^3\right]^{1/8}$ (Sari et al. 1998), where E is the isotropic equivalent energy of the jet and t is the time in the observer frame. By substituting these expressions in Equations (4)–(6), one derives

$$\nu_{\rm m} = 8.2\times10^{6}\left(1833f_{\rm p}\right)^{\frac{2}{p_1-1}}(37.2)^{\frac{1-q(2-p_1)}{p_1-1}} \times\frac{x_{\rm p}}{1+z}\xi^{\frac{-2(2-p_1)}{p_1-1}}\epsilon_{\rm e}^{\frac{2}{p_1-1}}\epsilon_{\rm B,-2}^{1/2} \times E_{52}^{\frac{p_1-q(2-p_1)}{4(p_1-1)}}n_0^{\frac{p_1-2+q(2-p_1)}{4}}\left(\frac{t_{\rm d}}{1+z}\right)^{\frac{-3\left[p_1-q(2-p_1)\right]}{4(p_1-1)}}{\rm Hz}, \quad (7)$$

$$\nu_{\rm c} = 1.5\times10^{15}\epsilon_{\rm B,-2}^{-3/2}E_{52}^{-1/2}n_0^{-1}\left[\frac{t_{\rm d}}{1+z}\right]^{-1/2}{\rm Hz}, \quad (8)$$

$$\nu_{\rm b} = 3.8\times10^{5}\ \frac{(6.1)^{1+2q}}{1+z}\xi^2\epsilon_{\rm B,-2}^{1/2}E_{52}^{\frac{1+q}{4}}n_0^{\frac{1-q}{4}} \times\left(\frac{t_{\rm d}}{1+z}\right)^{-\frac{3(1+q)}{4}}{\rm Hz}, \quad (9)$$

$$F_{\nu,\rm max} = 6.8\times10^{3}\phi_{\rm p}\epsilon_{\rm B,-2}^{1/2}E_{52}n_0^{1/2}d_{\rm L,28}^{-2}(1+z)\,\mu{\rm Jy}, \quad (10)$$

where $t_{\rm d}$ is the time in days. The coefficients in the above equations are somewhat different from those of Resmi & Bhattacharya (2008), since they considered the evolution of $\theta_{\rm j}$ due to the lateral expansion of the jet, though it is not important in the ultra-relativistic phase as discussed above.

The evolution of the synchrotron flux density at a given frequency (F_ν) relies on the order of the three break frequencies and the regime in which ν resides. For GRB 091127, the SED analysis requires $\nu_{\rm b}$ to evolve from $\nu_{\rm m} < \nu_{\rm opt} < \nu_{\rm b} < \nu_{\rm X} < \nu_{\rm c}$ to $\nu_{\rm m} < \nu_{\rm b} < \nu_{\rm opt} < \nu_{\rm X} < \nu_{\rm c}$ between $\sim$3 and $\sim$110 ks. Therefore, we just derive the flux density evolution in these regimes. For $\nu_{\rm m} < \nu < \nu_{\rm b} < \nu_{\rm c}$,

$$F_\nu = F_{\nu,\rm max}\left(\frac{\nu}{\nu_{\rm m}}\right)^{-\frac{p_1-1}{2}} \propto t^{-\frac{3}{8}(p_1+p_1q-2q)}. \quad (11)$$

For $\nu_{\rm m} < \nu_{\rm b} < \nu < \nu_{\rm c}$,

$$F_\nu = F_{\nu,\rm max}\left(\frac{\nu_{\rm b}}{\nu_{\rm m}}\right)^{-\frac{p_1-1}{2}}\left(\frac{\nu}{\nu_{\rm b}}\right)^{-\frac{p_2-1}{2}} \propto t^{-\frac{3}{8}(p_2+p_2q-2q)}. \quad (12)$$

We do not consider the flux evolution in the non-relativistic phase, as the light curves of GRB 091127 show no evidence of further steepening at later times, and we will show in Section 4 that the jet is still in the mildly relativistic phase at the end of the X-ray observations.

4. PARAMETER CONSTRAINT AND LIGHT CURVE FITTING

Before constraining the free parameters ($\epsilon_{\rm e}$, $\epsilon_{\rm B}$, ξ, E, and n), we summarize the decay slopes and spectral indices of the afterglow of GRB 091127. For the X-ray afterglow, the decay slopes $\alpha_{\rm X,1} = 1.02 \pm 0.04$, $\alpha_{\rm X,2} = 1.61 \pm 0.04$, the spectral index $\beta_{\rm X} = 0.75 \pm 0.004$. While for the optical afterglow (we do not use the fitting results in the NIR bands), the average decay slopes $\alpha_{\rm opt,1} = 0.38 \pm 0.04$, $\alpha_{\rm opt,2} \sim 1.6$, and the spectral index of $\beta_{\rm opt} = \beta_{\rm X} - 0.5 = 0.25 \pm 0.004$ is used according to the SED analysis. Both X-ray and optical/NIR light curves have an achromatic break at $t_{\rm bk} \approx 33$ ks. The spectral break frequency evolves as $\propto t^{-1.23\pm0.06}$.

At early times, $\nu_{\rm m} < \nu_{\rm opt} < \nu_{\rm b} < \nu_{\rm X} < \nu_{\rm c}$ is required, then the spectral indices of the electron energy distribution are given by $p_1 = 2\beta_{\rm opt} + 1 = 1.5 \pm 0.01$ and $p_2 = 2\beta_{\rm X} + 1 = 2.5 \pm 0.01$. With these values and according to Equations (9), (11), and (12), the decay indices of $\nu_{\rm b}$, $F_{\nu_{\rm opt}}$, and $F_{\nu_{\rm X}}$ are only functions of q. Therefore, the value of q is overconstrained. As the initial decay slope of the optical afterglow was not well fitted (Filgas et al. 2011), we use the decay indices of $\nu_{\rm b}$ and $F_{\nu_{\rm X}}$ to constrain q and give a consistency check using the optical data. With Equations (9) and (12) and the observed decay indices, we get

$$\frac{3(1+q)}{4} = 1.23 \pm 0.06, \quad (13)$$

$$\frac{3}{8}(p_2 + p_2q - 2q) = 1.02 \pm 0.04. \quad (14)$$

From Equations (13) and (14), we obtain $q = 0.64 \pm 0.08$ and $q = 0.44 \pm 0.21$, respectively. However, the former is preferred, since the left-hand side of Equation (13) is much more dependent on q than that of Equation (14). With this value of q and according to Equations (11) and (12), the derived decay indices are $\alpha_{\rm opt,1} = 0.44 \pm 0.02$ and $\alpha_{\rm X,1} = 1.06 \pm 0.02$, which are consistent with the observed values within 1σ errors. Therefore, we adopt $q = 0.64$ in the following calculations.

The synchrotron flux in the optical bands is given by

$$F_{\nu_{\rm opt}} = F_{\nu,\rm max}\left(\frac{\nu_{\rm opt}}{\nu_{\rm m}}\right)^{-\beta_{\rm opt}} = 263.9\ \xi_4^{-1/2}\epsilon_{\rm e,-1}\epsilon_{\rm B,-2}^{5/8}E_{52}^{1.15}n_0^{0.48}t_{\rm d}^{-0.44}\left(\frac{\nu_{\rm opt}}{\nu_{\rm r}}\right)^{-\beta_{\rm opt}}\mu{\rm Jy}. \quad (15)$$

By requiring the r-band flux be 827 μJy at 4000 s, we obtain

$$\xi_4^{-1/2}\epsilon_{e,-1}\epsilon_{B,-2}^{5/8}E_{52}^{1.15}n_0^{0.48}=0.8. \quad (16)$$

According to the SED analysis, ν_b should be $\sim$28.7 eV at 3404 s (Filgas et al. 2011), then with Equation (9), we have

$$\xi_4^2\epsilon_{B,-2}^{1/2}E_{52}^{-0.41}n_0^{0.1}=0.05. \quad (17)$$

Finally, ν_c should not have crossed the X-band at the last measurement of the X-ray afterglow, i.e., $\nu_c(4\times10^6\,\mathrm{s})>10$ keV. With Equation (9), we get

$$\epsilon_{B,-2}^{-3/2}E_{52}^{-1/2}n_0^{-1}>1.4\times10^4. \quad (18)$$

From Equations (16)–(18), one derives

$$\epsilon_{B,-2}n_0^{2/3}=0.28\epsilon_{e,-1}^{-4/3}E_{52}^{-1.4}, \quad (19)$$

$$\xi_4=0.22\ \epsilon_{B,-2}^{-1/4}E_{52}^{0.21}n_0^{-0.05}, \quad (20)$$

$$\epsilon_{e,-1}>45.6E_{52}^{-0.8}. \quad (21)$$

By requiring $\epsilon_e<1$ and a not-too-low efficiency of the prompt radiation (we simply assume $\eta_\gamma=E_\gamma/(E_\gamma+E)>5\%$), we derive $6.6<E_{52}<20.9$ and $\epsilon_{e,-1}>4.2$ from Equation (21). Here we take $E_{52}=20$ and $\epsilon_{e,-1}=4.5$. By substituting these values in Equation (19), we get $\epsilon_{B,-2}n_0^{2/3}=5.7\times10^{-4}$. The values of ϵ_B and n cannot be well constrained since both of them are highly uncertain parameters and vary over several orders of magnitude. Without loss of generality, we adopt $n_0=1$, then we obtain $\epsilon_{B,-2}=5.7\times10^{-4}$. By substituting these values in Equation (20), we get $\xi_4=2.7$. The value of ξ can be well constrained; it is around 2×10^4, varying within a factor of two, since it is weakly dependent on other parameters according to Equation (20).

We note that the value of ϵ_B obtained above is much smaller than the usually assumed ($\sim10^{-3}$–10^{-2}). However, such a small value may be more common according to the recent statistic results given by Santana et al. (2014). Using X-ray and optical afterglow observations, they found the distribution of ϵ_B has a range of $\sim10^{-8}$–10^{-3} with a median value of $\sim$ a few $\times10^{-5}$. Another separate work using the radio data also supports this result (Barniol Duran 2014).

Since we interpret the achromatic break at t_{bk} as a jet break, we can estimate the half-opening angle of the jet according to $\theta_j\sim\gamma(t_{bk})^{-1}$, thus we have

$$\theta_j=9.4\ E_{52}^{-1/8}n_0^{1/8}\left(\frac{t_{bk,d}}{1+z}\right)^{3/8}\ \mathrm{deg}=3\overset{\circ}{.}9. \quad (22)$$

The bulk Lorentz factor at the end of the X-ray observations is $\gamma(4\times10^6\,\mathrm{s})=2.5$, which is still mildly relativistic. Therefore, our explanation of the afterglow of GRB 091127 in the relativistic case is self-consistent.

As a whole, the DPLH model can roughly explain the main property of the spectral evolution in the optical/NIR bands of GRB 091127. However, the analytic treatment of the flux evolution given by Equations (11) and (12) is still too simple to describe the detailed spectral evolution and the smooth break at around t_{bk} in the optical/NIR light curves, which requires a very smooth spectral break at ν_b. In fact, when the equal arrival time surface effect (ETS) of the relativistic ejecta is considered (Waxman 1997; Panaitescu & Mészáros 1998; Sari 1998), the spectral and temporal breaks are rather smooth (Granot et al. 1999; Huang et al. 2007) and can be described by a smoothly broken power law at the spectral break (Granot & Sari 2002). Besides, for a uniform jet with a sharp cutoff at the edge, the jet break caused by the edge effect is very sharp as well. For GRB 091127, the predicted decay slope after the jet break is $\sim$1.8, which is still too steep compared with the observed value ($\sim$1.6). However, the more realistic jet may be structured (Rossi et al. 2002; Zhang & Mészáros 2002; Granot & Kumar 2003; Pescalli et al. 2015; Salafia et al. 2015), which could smoothen the jet break.

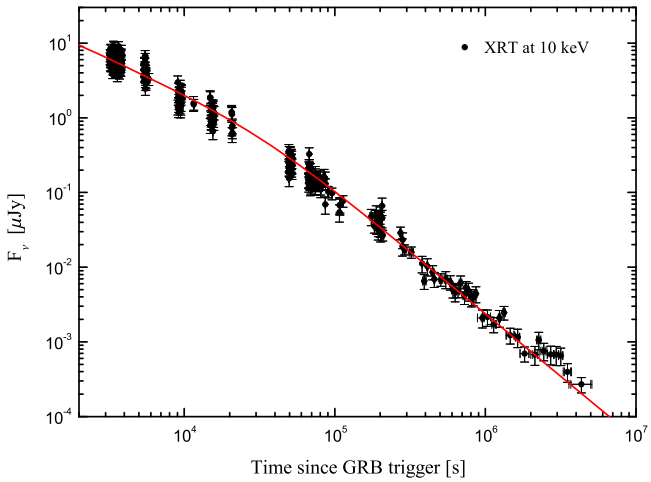

Figure 1. Fit of the X-ray light curve at 10 keV. The data (filled circles) are taken from http://www.swift.ac.uk/xrt_curves/00377179/ (Evans et al. 2009a). The solid line is the theoretical light curve given by Equation (23).

Therefore, instead of using Equations (11) and (12), we fit the multi-band light curves with the following expression

$$F_\nu=F_0\left[\left(\frac{\nu}{\nu_b}\right)^{s_1\beta_{opt}}+\left(\frac{\nu}{\nu_b}\right)^{s_1\beta_X}\right]^{-\frac{1}{s_1}}\left[1+\left(\frac{t}{t_{bk}}\right)^{s_2\Delta\alpha}\right]^{-\frac{1}{s_2}}, \quad (23)$$

where the first smoothly broken power law describes the spectral evolution with a smooth break ν_b, while the second describes the smooth jet break caused by the jet-edge effect. F_0 is the normalization, which can be obtained by requiring $F_{\nu_r}(4000\,\mathrm{s})=827$ μJy. s_1 and s_2 are smoothness parameters, we take $s_1=2.2$ according to the SED fitting (Filgas et al. 2011), and take $s_2=2$ to describe the sharpness of the X-ray light curve at t_{bk}. The parameter $\Delta\alpha=3/4$ accounts for the slope difference before and after the jet break. Here we still use ν_b given by Equation (9) with the parameters obtained above and neglect the small correction due to the ETS effect.

As can be seen from Figures 1 and 2, except for the SN components with which we are not concerned here, the multi-band afterglow light curves of GRB 091127 can be well fitted by our theoretical motivated equation of (23). This is to be expected, though, since the first smoothly broken power law in this fitting function is just the one used by Filgas et al. (2011) in their SED analysis. However, we give a physical meaning of the observed spectral break in this paper, which is expressed by Equation (9) instead of a free parameter in their SED fitting.

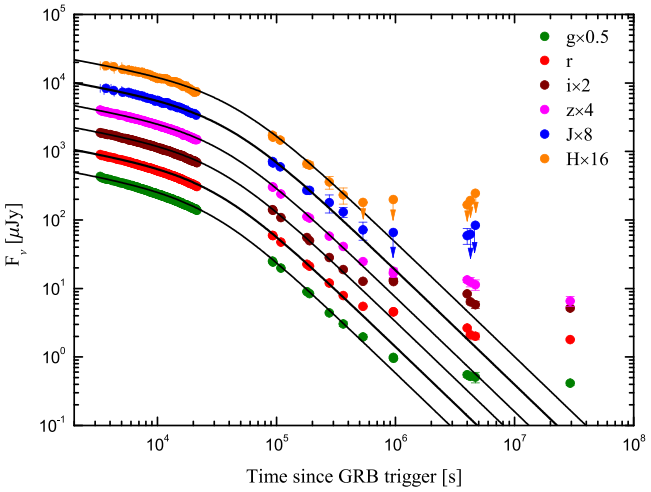

Figure 2. Fit of the multi-band optical/NIR light curves observed by GROND. The observational data (filled circles) are taken from Filgas et al. (2011). Adjacent light curves have been offset by a factor of two for clarity with r band unscaled. The solid lines are theoretical light curves given by Equation (23).

5. CONCLUSION AND DISCUSSION

GRB 091127, for which well-sampled broad-band afterglow data exist, shows evidence of a hard electron spectrum and strong spectral evolution with a spectral break moving from high to lower energies. The spectral break evolves much faster than the cooling break even in the ISM case, which challenges the standard afterglow model. In this paper, using the DPLH model and an assumed evolution function of the injection break, we interpreted the observed spectral break as the injection break frequency. The observed spectral evolution is due to this injection break crossing the optical/NIR bands. In addition, we interpreted the achromatic break at around 33 ks as a jet break caused by the jet-edge effect. We have shown that the multi-band observational data can be satisfactorily fitted in our framework.

Our model is intrinsically different from that of Filgas et al. (2011), although both assumed a hard electron spectrum. Filgas et al. (2011) used the SPLH model, they interpreted the observed spectral break as the cooling break, but required ϵ_B to evolve with time, while we used the DPLH model and explained the observed spectral break as the injection break without requiring evolving microphysical parameters. Currently, we have little knowledge of the injection break and its evolution, and in-depth numerical simulation studies on the electron acceleration process may help to solve these issues.

Resmi & Bhattacharya (2008) used the same model to explain the afterglows of three pre-*Swift* GRBs. However, the parameters of GRB 091127 are much different from those given by Resmi & Bhattacharya (2008). First, the optical spectral indices of their sample are in the range of 0.6–0.9. To be modeled with a hard electron spectrum, all the cooling frequencies ν_c of their sample were assumed to be below the optical band at the beginning of observations. In our study, the cooling break of GRB 091127 was required to be above the X-ray band even at late times. Second, all their injection break frequencies ν_b were assumed to be above the X-ray band, while for GRB 091127, ν_b was required to be between the optical and X-ray band at early times and to cross the optical band at later times. Third, since $\nu_c \propto \epsilon_B^{-3/2}$ and $\nu_b \propto \epsilon_B^{1/2}$, the relatively low ν_c and high ν_b determine that their derived ϵ_B ($\sim$0.01–0.2) is much larger than ours ($\sim 10^{-6}$–10^{-5}). Finally, all their values of q are lager than 1, while for GRB 091127, q is smaller ($\sim$0.6). Due to these differences among parameters, the afterglow of GRB 091127 reveals much different properties from those in Resmi & Bhattacharya (2008). In this case, we see the evolution of the injection break for the first time.

Besides GRB 091127, the other two GRB afterglows observed by the *Swift* satellite—GRB 060908 (Covino et al. 2010) and GRB 140515A (Melandri et al. 2015)—also show very flat spectra in the optical band ($\beta_{opt} \sim 0.3$) and could be explained with a hard electron spectrum (Wang et al. 2012; Melandri et al. 2015). Such GRBs, however, are still lacking. More observations of GRB afterglows with a hard electron spectrum and further developments in the area of simulations of the *Fermi* acceleration process in relativistic shocks will help us understand the origin of the hard electron distribution.

We acknowledge the anonymous referee for helpful comments and suggestions. We thank Tan Lu for encouraging support. Our work made use of data supplied by the UK *Swift* Science Data Centre at the University of Leicester. This study was supported by the National Basic Research Program of China with Grant No. 2014CB845800 and by the National Natural Science Foundation of China with Grants No. 11473012, No. 11475085, and No. 11275097.

REFERENCES

Achterberg, A., Gallant, Y. A., Kirk, J. G., & Guthmann, A. W. 2001, MNRAS, 328, 393
Band, D., Matteson, J., Ford, L., et al. 1993, ApJ, 413, 281
Baring, M. G. 2004, NuPhS, 136, 198
Barniol Duran, R. 2014, MNRAS, 442, 3147
Bednarz, J., & Ostrowski, M. 1998, PhRvL, 80, 3911
Beuermann, K., Hessman, F. V., Reinsch, K., et al. 1999, A&A, 352, L26
Bhattacharya, D. 2001, BASI, 29, 107
Bhattacharya, D., & Resmi, L. 2004, in ASP Conf. Ser. 312, Evolution of an Afterglow with a Hard Electron Spectrum, ed. M. Feroci et al. (San Francisco, CA: ASP), 411
Björnsson, G., Hjorth, J., Pedersen, K., & Fynbo, J. U. 2002, ApJL, 579, L59
Blandford, R. D., & McKee, C. F. 1976, PhFl, 19, 1130
Butler, N. R., Marshall, H. L., Ricker, G. R., et al. 2003, ApJ, 597, 1010
Cannizzo, J. K., Gehrel, N., & Vishniac, E. T. 2004, ApJ, 601, 380
Chevalier, R. A., & Li, Z.-Y. 2000, ApJ, 536, 195
Cobb, B. E., Bloom, J. S., Perley, D. A., et al. 2010, ApJ, 711, 641
Covino, S., Campana, S., Conciatore, M. L., et al. 2010, A&A, 521, A53
Covino, S., Malesani, D., Tavecchio, F., et al. 2003, A&A, 404, L5
Cowsik, R., Prabhu, T. P., Anupama, G. C., et al. 2001, BASI, 29, 157
Cucchiara, A., Fox, D., Levan, A., et al. 2009, GCN, 10202, 1
Curran, P. A., Evans, P. A., de Pasquale, M., Page, M. J., & van der Horst, A. J. 2010, ApJL, 716, L135
Curran, P. A., Starling, R. L. C., van der Horst, A. J., & Wijers, R. A. M. J. 2009, MNRAS, 395, 580
Dai, Z. G., & Cheng, K. S. 2001, ApJL, 558, L109
Dai, Z. G., & Lu, T. 1998, A&A, 333, L87
de Colle, F., Ramirez-Ruiz, E., Granot, J., & Lopez-Camara, D. 2012, ApJ, 751, 57
Evans, P. A., Beardmore, A. P., & Page, K. L. 2009a, MNRAS, 397, 1177
Evans, P. A., Page, K. L., & Troja, E. 2009b, GCN, 10201, 1
Fermi, E. 1954, ApJ, 119, 1
Filgas, R., Greiner, J., Schady, P., et al. 2011, A&A, 537, A57
Granot, J., & Kumar, P. 2003, ApJ, 591, 1086
Granot, J., Miller, M., Piran, T., Suen, W. M., & Hughes, P. A. 2001, in Era ESO Afterglow Symp., Gamma-ray Bursts in the Afterglow, Relativistic Jet, ed. E. Costa, F. Frontera & J. Hjorth (Berlin: Springer), 312
Granot, J., & Piran, T. 2012, MNRAS, 421, 570
Granot, J., Piran, T., & Sari, R. 1999, ApJ, 513, 679
Granot, J., & Sari, R. 2002, ApJ, 568, 820
Huang, Y. F., Cheng, K. S., & Gao, T. T. 2006, ApJ, 637, 873

Huang, Y. F., Gou, L. J., Dai, Z. G., & Lu, T. 2000, ApJ, 543, 90
Huang, Y. F., Lu, Y., Wong, A. Y. L., & Cheng, K. S. 2007, ChJAA, 7, 397
Ioka, K., Toma, K., Yamazaki, R., & Nakamura, N. 2006, A&A, 458, 7
Kirk, J. G., Guthmann, A. W., Gallant, Y. A., & Achterberg, A. 2000, ApJ, 542, 235
Kong, S. W., Wong, A. Y. L., Huang, Y. F., & Cheng, K. S. 2010, MNRAS, 402, 409
Kumar, P., & Granot, J. 2003, ApJ, 591, 1075
Kumar, P., & Zhang, B. 2015, PhR, 561, 1
Lemoine, M., & Pelletier, G. 2003, ApJL, 589, L73
Masetti, N., Palazzi, E., Pian, E., et al. 2001, A&A, 374, 382
Melandri, A., Bernardini, M. G., D'Avanzo, P., et al. 2015, arXiv:1506.03079
Mészáros, P., & Rees, M. J. 1993, ApJ, 405, 278
Mészáros, P., & Rees, M. J. 1997, ApJ, 476, 232
Mészáros, P., & Rees, M. J. 1999, MNRAS, 306, L39
Misra, K., Resmi, L., Pandey, S. B., Bhattacharya, D., & Sagar, R. 2005, BASI, 33, 487
Nousek, J. A., Kouveliotou, C., Grupe, D., et al. 2006, ApJ, 642, 389
Panaitescu, A., & Kumar, P. 2001a, ApJL, 560, L49
Panaitescu, A., & Kumar, P. 2001b, ApJ, 554, 667
Panaitescu, A., & Kumar, P. 2002, ApJ, 571, 779
Panaitescu, A., & Mészáros, P. 1998, ApJL, 493, L31
Panaitescu, A., Mészáros, P., Burrows, D., et al. 2006, MNRAS, 369, 2059
Pescalli, A., Ghirlanda, G., Salafia, O., et al. 2015, MNRAS, 447, 1911
Rees, M. J., & Mészáros, P. 1992, MNRAS, 258, 41P
Rees, M. J., & Mészáros, P. 1998, ApJL, 496, L1
Resmi, L., & Bhattacharya, D. 2008, MNRAS, 388, 144
Rhoads, J. E. 1999, ApJ, 525, 737
Rossi, E., Lazzati, D., & Rees, M. J. 2002, MNRAS, 332, 945
Sagar, R., Stalin, C. S., Bhattacharya, D., et al. 2001, BASI, 29, 91
Salafia, O. S., Ghisellini, G., Pescalli, A., Ghirlanda, G., & Nappo, F. 2015, MNRAS, 450, 3549
Santana, R., Barniol Duran, R., & Kumar, P. 2014, ApJ, 785, 29
Sari, R. 1998, ApJL, 494, L49
Sari, R., & Mészáros, P. 2000, ApJL, 535, L33
Sari, R., Piran, T., & Halpern, J. P. 1999, ApJL, 519, L17
Sari, R., Piran, T., & Narayan, R. 1998, ApJL, 497, L17
Shen, R., Kumar, P., & Robinson, E. L. 2006, MNRAS, 371, 1441
Smith, R. J., Kobayashi, S., Guidorzi, C., & Mundell, C. G. 2009, GCN, 10192, 1
Spitkovsky, A. 2008, ApJL, 682, L5
Stamatikos, M., Barthelmy, S. D., Baumgartner, W. H., et al. 2009, GCN, 10197, 1
Stanek, K. Z., Garnavich, P. M., Jha, S., et al. 2001, ApJ, 563, 592
Starling, R. L. C., Van der Horst, A. J., Rol, E., et al. 2008, ApJ, 672, 433
Thöne, C. C., Goldoni, P., Covino, S., et al. 2009, GCN, 10233, 1
Troja, E., Barthelmy, S. D., Baumgartner, W. H., et al. 2009, GCN, 10191, 1
Troja, E., Sakamoto, T., Guidorzi, C., et al. 2012, ApJ, 761, 50
Updike, A., Rossi, A., Rau, A., et al. 2009, GCN, 10195, 1
van der Horst, A. J., Paragi, Z., de Bruyn, A. G., et al. 2014, MNRAS, 444, 3151
van Eerten, H., van der Horst, A., & MacFadyen, A. 2012, ApJ, 749, 44
Wang, Y., Fan, Y.-Z., Wei, D.-M., & Stefano, C. 2012, ChA&A, 36, 148
Waxman, E. 1997, ApJL, 491, L19
Wijers, R. A. M. J., & Galama, T. J. 1999, ApJ, 523, 177
Zhang, B., Fan, Y. Z., Dyks, J., et al. 2006, ApJ, 642, 354
Zhang, B., & Mészáros, P. 2001, ApJL, 552, L35
Zhang, B., & Mészáros, P. 2002, ApJ, 571, 876
Zhang, W., & MacFadyen, A. 2009, ApJ, 698, 1261